Mater. Res. Soc. Symp. Proc. Vol. 911 © 2006 Materials Research Society 0911-B05-24

The Formation Mechanism of Carrot Defects in SiC Epifilms

Hui Chen, Guan Wang, Yi Chen, Xiaoting Jia, Jie Bai, and Michael Dudley
Department of Materials Science and Engineering, Stony Brook University, Stony Brook, NY. 11794-2275

ABSTRACT

Carrot-like defects in a 7° off-cut (from [0001] toward $<1\bar{2}10>$ direction) 4H-SiC wafer with a 36μm thick 4H-SiC epilayer have been investigated using Nomarski optical microscopy, synchrotron white beam x-ray topography (SWBXT), scanning electron microscopy (SEM) and transmission electron microscopy (TEM). X-ray topographs confirm that threading screw dislocations are often associated with the carrots. Cross-sectional TEM observation confirms that a prismatic stacking fault exists below the carrot. This fault was found to show contrast in all observed diffraction geometries except for g=0004. A model for the mechanism of formation of this type of defect during epitaxial growth is proposed.

INTRODUCTION

The growth of SiC using CVD has experienced great progress in the last decade. Defect densities in PVT grown 4H-SiC substrates have dramatically decreased and as a consequence so have those in CVD grown homoepitaxial layers particularly when grown on off-axis substrates. However, when growth is carried out on off-axis substrates, triangular 3C inclusions have been found to be a persistent problem[1-3] as have surface morphological defects that have a shape similar to a "carrot" (hereafter simply referred to as carrots)[3-6] and both are found to have significantly adverse effects on device performance[7]. Several groups[4-6] have studied carrot defects and found that they comprise complicated intersections of stacking faults on the prismatic and basal planes. However, while the general morphology of the defect may be understood to a certain extent, the formation mechanism of the carrots remains unclear. In this paper, we report on observations of these defects using SWBXT, SEM, and TEM and propose a model for their formation during epitaxial growth.

EXPERIMENTAL DETAILS

SWBXT experiments were carried out at the Stony Brook Topography Facility (Beamline X-19C) at the National Synchrotron Light Source, at Brookhaven National Laboratory. The white x-ray spectrum ranges from 0.01Å to 2.00Å, with peak intensity at around 0.8 Å. The specimen-film distances were set to be 25cm to reduce background noise. Three cross-sectional TEM samples containing carrot defects were made from a 2-inch 4H-SiC wafer with a 36μm-thick 4H-SiC homoepitaxial layer (substrate grown at II-VI WBG Inc, epilayer grown at SemiSouth). They were cut with angles of 90°, 60° and 30°, respectively, to the long axis of the carrot. Samples were mechanically ground using a T-tool and 30 μm, 15 μm, 6 μm, 3 μm, 1 μm and 0.5 μm diamond lapping films and then ion milled to electron transparency. TEM observation was carried out on a Philips CM12 transmission electron microscope with an accelerating voltage of 120KV.

RESULTS AND DISCUSSION

Fig. 1 shows SEM images of the surface morphology of typical carrot defects. Fig. 2 shows a grazing incidence topograph recorded from the same sample showing contrast from the carrot defects and confirming that a threading screw dislocation exists at the broader end of the carrot in agreement with previous reports. In this particular case, a linear array of carrots is distributed along what appears from detailed optical microscopy and topography studies to be a scratch at the substrate/epilayer interface.

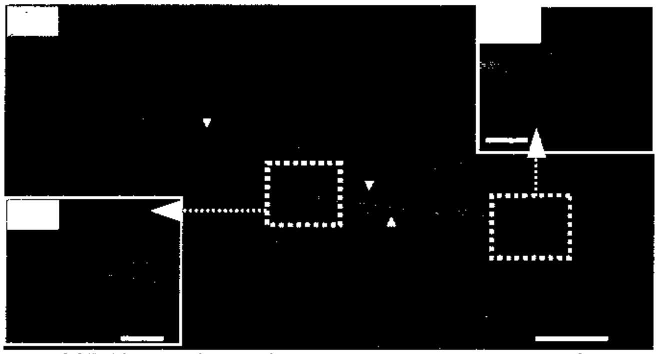

Figure 1. Back scattered SEM images of the surface morphology of typical carrot defects. (a) Morphological structure of the whole carrot. (b) Magnified image of the broader ends of carrot defects. (c) Magnified image of the narrower ends of carrot defects.

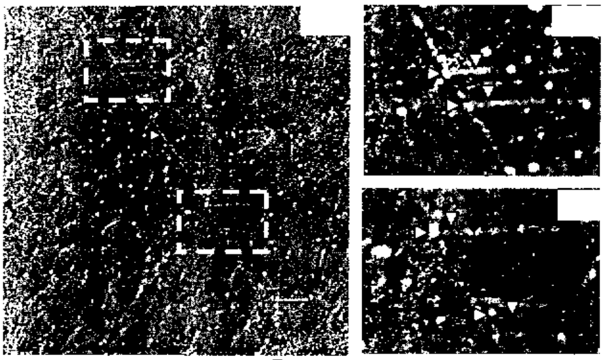

Figure 2. Grazing incidence x-ray topograph ($g = 1\bar{2}18$) of a local area containing carrot defects. (a) A row of carrot defects aligned along a scratch at the substrate/epilayer interface. (b) Magnified topograph of the dotted framed region A in Fig.(a). (c) Magnified topograph of the dotted enframed region B in Fig.(a). (SD: threading screw dislocation)

Based on correlated cross-sectional Lang topography and KOH etching studies, as well as cross-sectional TEM studies, Benamara[6] proposed a model for the three dimensional configuration for the defects lying beneath the surface feature that constitutes the carrot.[6] The small ridge running along the axis of the carrot was portrayed as the surface intersection of a stacking fault lying on the prismatic plane which was bounded on one side by a deflected threading screw dislocation and on the other by the stair rod dislocation which was found at the intersection between the fault on the prismatic plane and another on the basal plane. The basal plane fault, which fanned out from the intersection of the original screw dislocation and the substrate epilayer interface was bounded on its other side by a partial dislocation.

Insight into the possible formation mechanism of such a structure can be found by considering the nature of the substrate surface prior to epilayer growth. Substrate surfaces are typically hydrogen etched which can produce complicated step structures at the surface intersections of screw dislocations. The hydrogen etching process can be considered to resemble reverse crystal growth in that atoms are removed preferentially from the vertical step risers present on the substrate surface. Such vertical step risers also exist at the surface intersections of screw dislocations and hydrogen etching can give rise to an unwinding of the surface growth spirals. Meanwhile, it is well known that basal plane dislocations, which are often dissociated into two Shockley partials separated by a stacking fault, interact strongly with the screw dislocations, being pinned by them while bowing out under stress. Since these latter processes occur throughout the substrate volume, it is possible that some of them occur close to the substrate surface and that during hydrogen etching all or part of the intersection of a pair of partial dislocations on the vertical step riser close to the core of a screw dislocation spiral may be exposed.

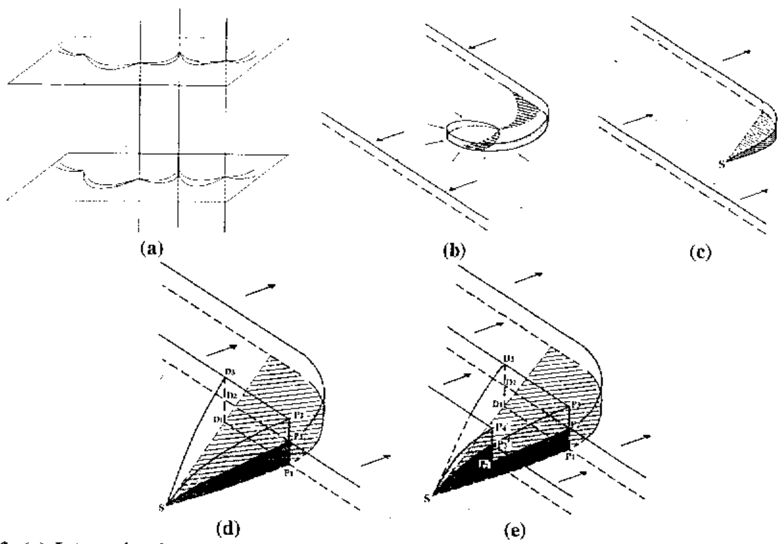

Figure 3. (a) Interaction between dissociated basal plane dislocations moving under stress and threading screw dislocations. (b)-(f) Interaction between the surface intersection of a dissociated basal plane dislocation with a screw dislocation and advancing vicinal steps.

Figure 3(a) show how the dissociated basal plane dislocations are pinned by the threading screw dislocations and constrict at the pinning points. The intersection close to the substrate surface between a basal plane dislocation separated into its two partials and a screw dislocation is shown schematically in Fig. 3(b), which shows how hydrogen etching could potentially expose a faulted region of crystal in the region of growth spiral close to the dislocation core. Once epilayer growth is initiated, the flow of vicinal steps will tend to overwhelm the flow of steps associated with the growth spiral. As this occurs, the advancing vicinal steps eventually reach the region close to the core of the growth spiral and a segment of vertical step riser which runs parallel to the vicinal step flow direction (Fig.3(c)) at which point the advancing vicinal step is forced to split, with one side riding up to the left (replicating the dislocation) while the other meets the vertical step riser exposed near the dislocation core. The vertical step riser near the core, SP_1P_2, exposes a faulted structure (Fig.3(d)) corresponding to the original structure displaced by the exited leading Shockley partial of the pair (actually the whole volume $SD_1D_3P_3P_1$ is faulted). This displacement is confined to the basal plane. It is envisaged that the strain field associated with the screw dislocation can give rise to an additional shift, parallel to the c-axis. Considering that the displacement of regions diametrically opposed across the dislocation core is c/2 then one might expect this to be the magnitude of the shift (c/4 is also possible in this structure). This means that the total displacement of the vertical step riser exposed on the portion of growth spiral close to the dislocation core is the sum of the Shockley partial displacement and c/2 (or c/4). As this riser meets with the inside face of the lower portion of the split advancing vicinal step, a fault, SP_1P_2, will be formed in the plane parallel to the step flow direction (in this case the prismatic plane, shown in enlarged view in Fig.3(e)). The original basal plane fault, SD_1P_1, is bounded on one side by the trailing partial SD_1 and on its other side by a stair rod dislocation, SP_1, at the intersection between the fault on the prismatic plane and the basal plane fault. The trailing partial will continue on its original trajectory as it is replicated as will the stair rod dislocation. As the riser $D_1P_1P_2D_2$ advances (Fig. 3(d)) the basal plane fault is further replicated. The process repeats itself as the next vicinal step advances over the faulted dislocation core as shown in Fig. 3(e), replicating another region of prismatic stacking fault, $SP'_2P'_3$ and exposing another region of step riser $SP'_3P'_4$ at the dislocation core. The prismatic plane fault will be bounded at one end by the screw dislocation which may be slightly deflected towards the step flow direction by the effects of image force. It is believed that this overall scenario can lead to a configuration of faults similar to that proposed by Benamara *et al*[6].

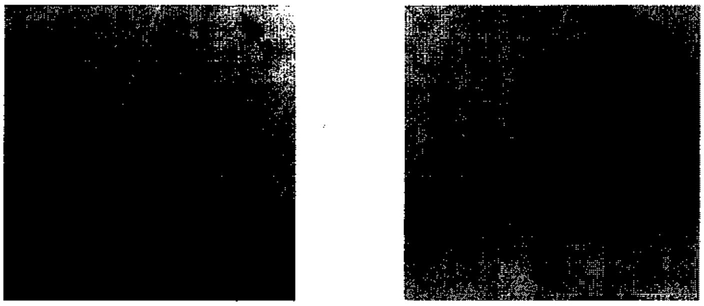

(a) (b)

Figure 4. TEM dark field images of the prismatic fault. (a) $g=10\bar{1}6$; (b) $g=10\bar{1}2$

Table I. Possible prismatic fault vectors

	$1/3\langle 0\bar{1}10\rangle^{c}$	$1/3\langle \bar{1}100\rangle^{c}$
$1/4\langle 0001\rangle^{a}$	$1/12\langle 0\bar{4}43\rangle^{d}$	$1/12\langle 4\bar{4}03\rangle^{d}$
$1/4\langle 0001\rangle^{a}+1/6\langle 10\bar{1}0\rangle^{b}$	Unfavorable bonding	$1/12\langle 6\bar{4}\bar{2}3\rangle^{d}$
$1/4\langle 0001\rangle^{a}+1/6\langle \bar{1}100\rangle^{b}$	Unfavorable bonding	$1/4\langle 2\bar{2}01\rangle^{d}$
$1/4\langle 0001\rangle^{a}+1/6\langle 01\bar{1}0\rangle^{b}$	Unfavorable bonding	$1/12\langle 4\bar{2}\bar{2}3\rangle^{d}$
$1/2\langle 0001\rangle^{a}$	Unfavorable bonding	$1/6\langle 2\bar{2}03\rangle^{d}$
$1/4\langle 0001\rangle^{a}+1/6\langle 0\bar{1}10\rangle^{b}$	$1/4\langle 0\bar{2}21\rangle^{d}$	Unfavorable bonding
$1/4\langle 0001\rangle^{a}+1/6\langle \bar{1}100\rangle^{b}$	$1/12\langle \bar{2}\bar{2}43\rangle^{d}$	Unfavorable bonding

a: displacement vector along c-axis; b: additional shift; c: Shockley partial shift; d: resultant fault vector

There are several different possible Burgers vectors for the dissociated basal plane dislocation and Shockley fault which can lead to different possibilities for the prismatic plane fault vector. Preliminary TEM observations (examples are shown in Fig.4) indicate that the fault on the prismatic plane is clearly visible on all reflections except for g=0004 (this is consistent with previously reported observations). In the case of prismatic faults on $[1\bar{2}10]$ in GaN[8], an additional half Shockley partial shift is energetically favored, which transforms the stacking mismatch boundary into a prismatic stacking fault with fault vector of $1/2\langle 10\bar{1}1\rangle$ type. In our case, different Shockley partial shifts (with or without additional half Shockley partial shifts) were analyzed and combined with c/2 (or c/4) shifts depending on the structural geometry. Some of the possible prismatic fault vectors are listed in Table I after eliminating some unfavorable cases within which the atomic bonds are too long or short or involve atoms of the same kind. One of the possible fault vectors listed in Table I, $1/12\langle 6\bar{4}\bar{2}3\rangle$, is the same type as the possible fault vector $1/12\langle 4\bar{4}03\rangle+1/n\langle 10\bar{1}0\rangle$ postulated by Benamara *et al*[6] if a value of n=6 is chosen. Further work is underway to confirm these possible fault vectors.

The involvement of basal plane dislocations in the carrot formation mechanism is consistent with the observation that scratches at the substrate/epilayer interface can act as nucleation sites for the carrots (see Fig. 2) since locally high densities of basal plane dislocations are expected at surface scratches and therefore an enhanced probability of near surface interactions between basal plane dislocations and screw dislocations.

CONCLUSIONS

A model for the formation mechanism of the carrot defect is proposed. This model involves the hydrogen etching induced exposure of the interaction between a dissociated basal plane dislocation and a threading screw dislocation which exposes a faulted step riser at the core of the dislocation. As this faulted step riser is overgrown by advancing vicinal steps, the basal plane fault already present is converted into a fault on the prismatic plane with a stair rod dislocation existing at their junction. This structure is then replicated as the epilayer grows according to the step flow mechanism. This model appears consistent with present and previous observations of the defect structure observed beneath the carrot surface feature.

ACKNOWLEDGMENTS

The authors gratefully acknowledge bulk and epi crystal growth and provision of samples by the II-VI Incorporated and SemiSouth teams. All of the X-ray topography experiments have been carried out at Stony Brook Topography Facility (Beamline X19C) at the National Synchrotron Light Source (NSLS), Brookhaven National Laboratory, which is supported by the U.S. Department of Energy (D.O.E.).

REFERENCES

1. W. Si, M. Dudley, H. Kong, *et al.*, *J. Electron. Mater.*, **26**, 3 (1997).
2. T. Kimoto, N. Miyamoto and H. Matsunami, *IEEE Transactions on Electron Devices*, 46, 3 (1999).
3. T. Okada, T. Kimoto, Keita Yamai, *et.al.*, *Mater. Sci. &. Eng.*, **A361**, 67 (2003).
4. T. Okada, T. Kimoto, H. Noda, *et.al.*, *Jpn. J. Appl. Phys.*, **41**, 6320 (2002).
5. X. Zhang, S. Ha, M. Benamara, *et.al.*, *Appl .Phys.Lett.*, **85**, 22 (2004).
6. M. Benamara, X. Zhang, and M. Skowronski, *Appl .Phys.Lett.*, **86**, 021905 (2005).
7. Y. Wang, G. N. Ali, M. K. Mikhov, *et al.*, *J. Appl. Phys.*, **97**, 013540 (2005).
8. J. E. Northrup, *Appl. Phys. Lett.* **72**, 18 (1998).